Journal of the Mechanical Behavior of Biomedical Materials 76 (2017) 110–118

Contents lists available at ScienceDirect

Journal of the Mechanical Behavior of Biomedical Materials

journal homepage: www.elsevier.com/locate/jmbbm

Elevated temperature adhesion of bioinspired polymeric micropatterns to glass

Viktoriia Barreau[a,b], Dan Yu[a], René Hensel[a], Eduard Arzt[a,b,*]

[a] INM – Leibniz Institute for New Materials, Campus D2 2, 66123 Saarbrücken, Germany
[b] Department of Materials Science and Engineering, Saarland University, 66123 Saarbrücken, Germany

ARTICLE INFO

Keywords:
Adhesion
Micropatterning
Viscoelasticity
Glass transition temperature

ABSTRACT

Micropatterned polymer surfaces that operate at various temperatures are required for emerging technical applications such as handling of objects or space debris. As the mechanical properties of polymers can vary significantly with temperature, adhesion performance can exhibit large variability. In the present paper, we experimentally study temperature effects on the adhesion of micropatterned adhesives (pillar length 20 μm, aspect ratios 0.4 and 2) made from three different polymers, i.e., polydimethylsiloxane (PDMS), perfluoropolyether dimethacrylate (PFPEdma), and polyurethane (PU-ht). PU specimens showed the highest pull-off stresses of about 57 kPa at 60 °C, i.e., more than twice the value of unpatterned control samples. The work of separation similarly showed a maximum at that temperature, which was identified as the glass transition temperature, T_g. PDMS and PFPEdma specimens were tested above their T_g. As a result, the adhesion properties decreased monotonically (about 50% for both materials) for temperature elevation from 20 to 120 °C. Overall, the results obtained in our study indicate that the operating temperature related to the glass transition temperature should be considered as a significant parameter for assessing the adhesion performance of micropatterned adhesives and in the technical design of adhesion devices.

1. Introduction

Synthetic fibrillar dry adhesives are currently of great interest for enabling novel pick-and-place systems and other emerging applications. Particularly, their applicability even to rough substrate materials (Barreau et al., 2016) and the possible handling of fragile objects (Zhou et al., 2013) even in vacuum (Purtov et al., 2015) may pave the way for a new generation of handling and gripping systems. Over the last decade, several design parameters of fibrillar dry adhesives have been systematically studied (Del Campo et al., 2007; Greiner et al., 2007; Kroner and Arzt, 2012; Fischer et al., 2017). In general, splitting of an adhesive contact leads to better properties compared to an unpatterned, smooth adhesive contact because of a strong reduction of the elastic strain energy penalty for smaller contacts (size effect) (Arzt et al., 2003). Furthermore, contact splitting leads to an extrinsic contribution to the work of separation due to the interrupted crack propagation along the single contacts, an enhanced adaptability to rough substrates related to the higher compliance of the patterned surface, and a reduced sensitivity to defects compared to a single unpatterned contact (Kamperman et al., 2010). For the rational design of fibrillar adhesives, Spolenak et al. (2005) and Greiner et al. (2009) proposed maps that predict the optimal pillar geometry as function of the elastic properties and the tip shapes including limits such as cohesive strength, agglomeration of the fibrils, and the upper limit for the adhesion strength. Many additional parameters such as the stiffness of the substrate (Cheung and Sitti, 2009; Khaderi et al., 2015), elastic gradients inside the structures (Fischer et al., 2017; Balijepalli et al., 2017) or material viscoelasticity (Castellanos et al., 2011; Lakhera et al., 2013; Yu et al., 2013) have been studied experimentally and theoretically.

A critical issue that was neglected for micropatterned adhesives is the adverse effects of higher than ambient temperatures on adhesive properties. The mechanical properties of polymers drastically change with temperature, particularly if the temperature variation exceeds the glass transition temperature, T_g. At T_g, the molecular mobility changes from a glassy state ($T<T_g$) to a more flexible rubber state ($T>T_g$) with a simultaneous strong decrease of the elastic modulus. However, the adhesion performance is generally not a simple function of temperature: For an ideal contact situation, the higher modulus below T_g can enhance the adhesion properties of an adhesive film in contact with a rigid flat punch (Khaderi et al., 2015; Kendall, 1971). By contrast, a stiffer material will prevent intimate contact formation,

* Corresponding author at: INM – Leibniz Institute for New Materials, Campus D2 2, 66123 Saarbrücken, Germany.
E-mail address: eduard.arzt@leibniz-inm.de (E. Arzt).

http://dx.doi.org/10.1016/j.jmbbm.2017.04.007
Received 21 February 2017; Received in revised form 4 April 2017; Accepted 5 April 2017
Available online 07 April 2017
1751-6161/ © 2017 The Authors. Published by Elsevier Ltd. This is an open access article under the CC BY-NC-ND license (http://creativecommons.org/licenses/BY-NC-ND/4.0/).

particularly on a rough surface, and the diminished contact area can result in reduced adhesion. Above T_g, contact formation may be improved but the lower modulus can at the same time reduce the adhesion (Castellanos et al., 2011; Lakhera et al., 2013; Yu et al., 2013). For viscoelastic materials, viscoelastic losses additionally contribute to stiffness variations. Hence, the work of separation will increase when energy is dissipated in the system. At the glass transition temperature, the viscoelastic loss factor exhibits a maximum (Turi, 2012). Accordingly, Zosel measured the highest adhesion for pressure sensitive adhesives (PSAs) close to T_g Zosel (1985, 1991). Theoretically, energy dissipation due to viscoelastic losses at the crack tip will enhance the critical energy release rate necessary for crack propagation (Andrews and Kinloch, 1973; Barquins and Maugis, 1981; Greenwood and Johnson, 1981). In addition to interfacial dissipative processes, energy dissipation due to bulk deformation can contribute to enhanced adhesion, which occurs particularly in case of strong interfacial attraction (Crosby and Shull, 1999; Shull, 2002).

Detailed studies of bulk and interfacial contributions to the adhesion energy were performed by atomic force microscopy (AFM). For polydimethylsiloxane (PDMS), Awada et al. (2011) found, with increasing temperature (from 30 to 140 °C), a reduction in adhesion which they attributed to the decrease of intermolecular interactions due to higher thermal fluctuations (Noy et al., 2003). They further demonstrated that the adhesion energy at the nanoscale was a function of the thermodynamic work of adhesion (related to the surface free energies) and the dissipative energy, expressed by molecular mass and a dissipative coefficient, which depends on temperature and separation rate. Similar relationships were further established by experiments and so-called master curves showing the correlation between adhesion strength, temperature, and separation rate (Tsui et al., 2000; Cappella and Stark, 2006). Luengo et al. (1998) suggested a mechanism to describe the enhanced adhesion at T_g, where the enhanced mobility induces molecular rearrangements such as polymer chain entanglements across the interface, like molecular rearrangements occurring in bulk. In addition, inelastic surface deformations or bulk flow might contribute to energy dissipation at higher temperatures and lower rates (Zeng et al., 2006).

The materials used in the present study were polydimethylsiloxane (PDMS), polyurethane (PU-ht), and perfluoropolyether dimethacrylates (PFPEdma). All materials are highly cross-linked elastomers that exhibit a certain stability at elevated temperatures, which makes them interesting candidates for applications at elevated temperatures. PDMS, which has been widely used as a 'standard' material for micropatterned adhesives, decomposes thermally above 300 °C (Camino et al., 2001). PFPEdma exhibits considerable high temperature resistance due to the fluorine content of about 54 at% and can be applied at temperatures ranging from −50 °C to 290 °C. However, the material inherently exhibits a very low surface free energy and hydrophobicity (Hensel et al., 2012; Hensel et al., 2014); hence, its application for adhesives needs to be critically evaluated. In contrast, polyurethanes can exhibit very strong adhesion (Kim et al., 2007; Murphy et al., 2007), but show lower thermal stability (up to 150 °C) than the silicones and fluorinated polymers.

In the present paper, the adhesion of micropatterned polymer adhesives to a spherical glass probe was investigated at elevated temperatures up to 120 °C. The adhesion characteristics were evaluated in terms of pull-off stress and work of separation. The results obtained will be discussed in relation to thermally induced variations of the viscoelastic material properties.

2. Materials and methods

2.1. Microstructure fabrication

Micropatterned adhesive surfaces were fabricated from polydimethylsiloxane (PDMS, Sylgard 184 kit, Dow Corning), perfluoropolyether dimethacrylate (PFPEdma, Fomblin MD40, Solvay Solexis) and a high-temperature polyurethane, (PU-ht, U-835, Alfa Aesar) using replica molding. Master structures having hexagonal micropillar arrays with aspect ratio 2 and 0.4 (pillar length: 20 μm; pillar diameters: 10 and 50 μm, and a pitch twice the respective pillar diameter) and their corresponding PDMS molds were generated as described previously (Barreau et al., 2016). For the microstructures, the PDMS prepolymer (10 weight parts of the base to 1 weight part of the curing agent) was degassed under vacuum for 5 min. It was then filled into the mold, degassed for 10 min, and cured at 75 °C for 24 h in an oven. The PFPEdma and PU-ht oligomers were mixed with 0.5 wt-% 2-hydroxy-2 methyl-propiophenone (Sigma Aldrich) as a photoinitiator for UV-curing. The pre-polymer mixtures were poured into the mold and exposed to UV-light (365 nm, Omnicure S1500, Excelitas Technologies) under a nitrogen atmosphere for 5 min. Upon crosslinking, samples were carefully peeled off the molds. For a few analyses, PU-ht was thermally post-baked in addition to a prior UV-crosslinking at 120 °C for 15 min in an oven.

2.2. Adhesion measurements

The adhesion data presented in this paper were obtained by using a custom-built adhesion-measuring device, which is schematically shown in Fig. 1a. It consists of a pivotable stage, equipped with a heating element (PE120, Linkam), and a spherical glass probe with a curvature radius of 15 mm mounted on a flexible double beam glass spring. Forces were deduced from the beam deflection measured by a laser interferometer multiplied with its spring constant of 2240 N m^{-1}. Displacements reported correspond to the elongation of the micropatterned adhesives during retraction, i.e., they were calculated from the differential displacement of the stage relative to the deflected beam. The pull-off force (maximum tensile force) was determined from these

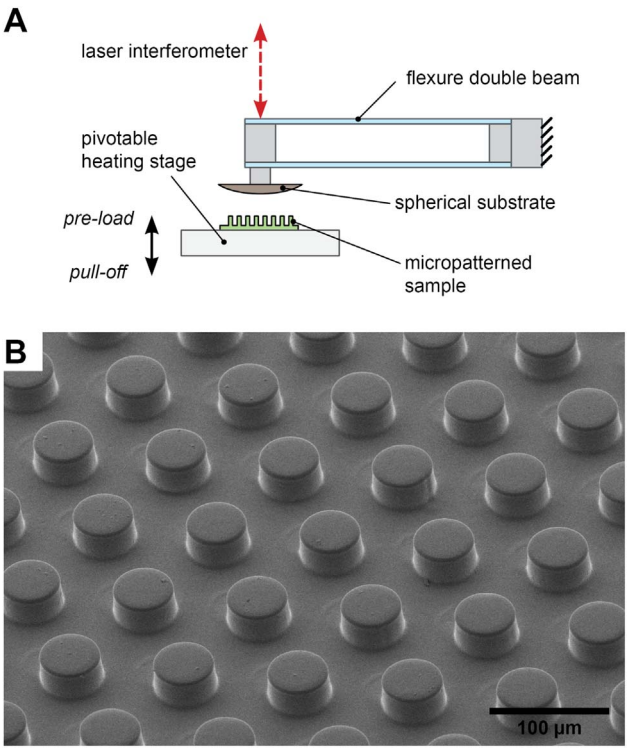

Fig. 1. Adhesion measurement and samples: (A) Schematic illustration of the adhesion measurement device that consists of a pivotable and heating stage for sample manipulation and a glass lens mounted on a flexible double beam. The laser interferometer monitors the elastic deflection of the beam, from which the forces are deduced. **(B)** Scanning electron micrograph of a representative micropatterned PDMS sample with pillars of length 20 μm and diameter 50 μm.

force-displacement curves. The pull-off stress was calculated by dividing the pull-off force by the apparent contact area. The apparent contact area was calculated according to a geometrical relationship based on the radius of the probe and the indentation depth obtained from the experiments (Greiner et al., 2007). The work of separation (area under the curve in the tensile regime) was determined from the stress-displacement curves. All measurements were performed at a constant compressive preload of 30 mN, at four different sample positions, at constant displacement velocity of 5 μm s^{-1}, and at a relative humidity of 45 ± 5%. The adhesion tests were conducted by increasing the temperature of the samples from 20 °C to 120 °C (heating rate: 20 °C min^{-1}) and subsequently decreasing the temperature from 120 °C to 20 °C (cooling rate: 20 °C min^{-1}) in increments of 20 °C. Before the adhesion measurements, the temperature was held constant for more than 15 min. The cooling process was initiated by flowing cold water through the heating stage. Each heating-cooling cycle was traversed three times.

2.3. Material analysis

The mechanical properties of all materials were studied by dynamic mechanical thermal analysis (DMTA, Q800, Waters GmbH). Cuboid polymer samples with dimensions $20 \times 12.5 \times 2.5$ mm^3 were fabricated and tested in the temperature range between −100 °C and 120 °C at a heating rate of 3 K min^{-1}. The glass transition temperature was determined from the maximum value of the viscoelastic loss factor, $\tan\delta$. All tests were performed under nitrogen atmosphere at an oscillatory frequency of 1.0 Hz in tensile mode. X-ray diffraction analysis (XRD, X'Pert MRD, PANalytical) was used to characterize the material microstructure of bulk PU-ht upon (a) UV-curing and (b) UV-curing with subsequent post-bake. As a source, Cu K-alpha was used (40 kV, 30 mA). The angle (2*theta) of the incident radiation was varied between 3° and 150° in increments of 0.02°. The Soller slit was set to 2.5° and an aperture of 0.5 was used. The diffraction patterns were analyzed in terms of constructive interference patterns due to crystalline domains in the polymer microstructure. Based on that, variations of the of the crystallinity before and after post-bake could be qualitatively compared.

2.4. Surface free energy measurement

The surface free energy of PU-ht was evaluated using a contact angle goniometer (OCA35, DataPhysics), equipped with analysis software SCA20. A flat film of PU-ht was prepared by coating a 120 μm thick layer of liquid PU-ht resin on PET foil and, subsequently, UV-cross-linking as described above. Contact angles of deionized water with surface tension of 72.3 mN/m and *n*-hexadecane with surface tension of 27.5 mN/m were measured and subsequently used to deduce the surface free energy value by Wu's Harmonic Mean Method (Wu, 1973).

3. Results

3.1. Adhesion measurements

Micropillar arrays generated from PDMS, PFPEdma and PU-ht are exemplarily shown in Fig. 1**b**. Fig. 2 shows the results obtained from adhesion measurements at different temperatures for the PDMS specimens. Typical force–displacement curves (tensile forces in retraction mode) of microstructures with a diameter of 10 μm at different temperatures are displayed in Fig. 2**a**. While the shapes of the curves were similar, the pull-off forces (maximum forces) and the displacements at pull-off decreased with increasing temperature by a factor of almost 2. Fig. 2**b** represents the decrease of the pull-off stress with increasing temperature for the patterned and unpatterned PDMS samples in three consecutive heating cycles. The highest pull-off stress of 3.4 kPa was obtained at 20 °C for the pillar diameter of 10 μm (aspect ratio 2). The values of the unpatterned control were slightly higher than the values for the pillar diameter of 50 μm (aspect ratio 0.4). This result is in line with our earlier study, where we detached similar PDMS microstructures from smooth and rough substrates (Barreau et al., 2016). Fig. 2**c** shows how the work of separation decreased with increasing temperature. Interestingly, this behavior is more strongly pronounced in the unpatterned control (from 3.4 to 0.3 mJ/m^2; i.e. a decrease by factor of 11) than for the micropatterned surface with pillar diameter 10 μm (from 12.8 to 3.6 mJ/m^2; i.e. a decrease by factor of 3.5). Thus, the reduction of the work to separate the adherents at higher temperatures could be decreased by surface patterning. Fig. 2**d** depicts the monotonic decrease of the pull-off stress and the maximum strain at detachment with increasing temperature; however, the apparent stiffness of the system (that is the slope of the secants; dotted lines) remained almost constant for the whole temperature range.

Fig. 3 shows the results of the adhesion measurements for the microstructures made from PFPEdma. The force-displacement curves for temperatures ranging from 20 to 60 °C exhibit almost identical profiles (Fig. 3**a**). At 80 °C, however, the pull-off force drops by factor 2 compared to the lower temperatures. At temperatures above 80 °C, the curves are again almost identical. The force-displacement curves were again similar for all heating cycles. The pull-off stresses of the PFPEdma specimens decreased only slightly from 20 to 60 °C but dropped to the half of the value (for pillar structures with 10 μm diameter) at temperatures of 80 °C and higher (Fig. 3**b**). Overall, the pull-off stress of the micropatterned PFPEdma specimens was almost one order of magnitude smaller than for the PDMS specimens. Fig. 3**c** shows a similar trend for the work of separation as a function of temperature. Interestingly, the pull-off stress and the work of separation obtained for the unpatterned PFPEdma control were almost equal to zero whereas the patterned specimens showed measurable adhesion. Hence, the highly-fluorinated polymer was intrinsically non-adhesive, but became slightly adhesive if patterned. The apparent stiffness of the adhesive dropped by a factor 2 for a temperature increase from 60 to 80 °C (Fig. 3**d**), while below and above this transition the stiffnesses were similar.

Fig. 4 shows the substantially different results for PU-ht. In the first heating cycle, the force-displacement curves reveal that the adhesion *increased* up to 60 °C, where the pull-off force and the displacement exhibited a maximum of about 5.5 mN and 3.8 μm, respectively (Fig. 4**a**). Above 60 °C, the adhesive forces dropped and reached 700 μN at 120 °C. In the second heating cycle, the specimens behaved much stiffer at temperatures below 80 °C; the stiffness (i.e. the slope of the force-displacement curve) increased by a factor 3 from about 1800 N m^{-1} to 5000 N m^{-1} for all samples measured from 20 to 60 °C. Interestingly, the maximum pull-off forces in that temperature range were similar in all heating cycles, whereas the displacements at pull-off were significantly reduced. The differences of the pull-off stress, strain at detachment, and the apparent stiffness between the first and the second heating cycle are further displayed in Fig. 4**d**. Hence, the overall stiffer structures in the second cycle are more adhesive. The results obtained in third heating cycle were almost identical to those obtained in the second cycle. At 100 and 120 °C, the force-displacement curves and stiffness of the specimens were similar for all three cycles. Fig. 4**b** shows the pull-off stresses of the PU-ht specimens, which exhibited values of roughly one order of magnitude higher than PDMS and two orders of magnitude higher than PFPEdma. PU-ht was the only material that showed an *increase* in adhesion up to 60 °C, where a maximum pull-off stress value was obtained for all cycles. Unlike the pull-off force in Fig. 4**a**, the pull-off stress was further enhanced by factor 6 in the second and third cycle; this is the result of the higher material stiffness in conjunction with a reduced contact area. The work of separation similarly exhibited a maximum value at 60 °C (Fig. 4**c**); however, in contrast to the pull-off stress, it was reduced by a factor of 2.5 (for microstructures with a diameter of 10 μm) upon the first heating cycle,

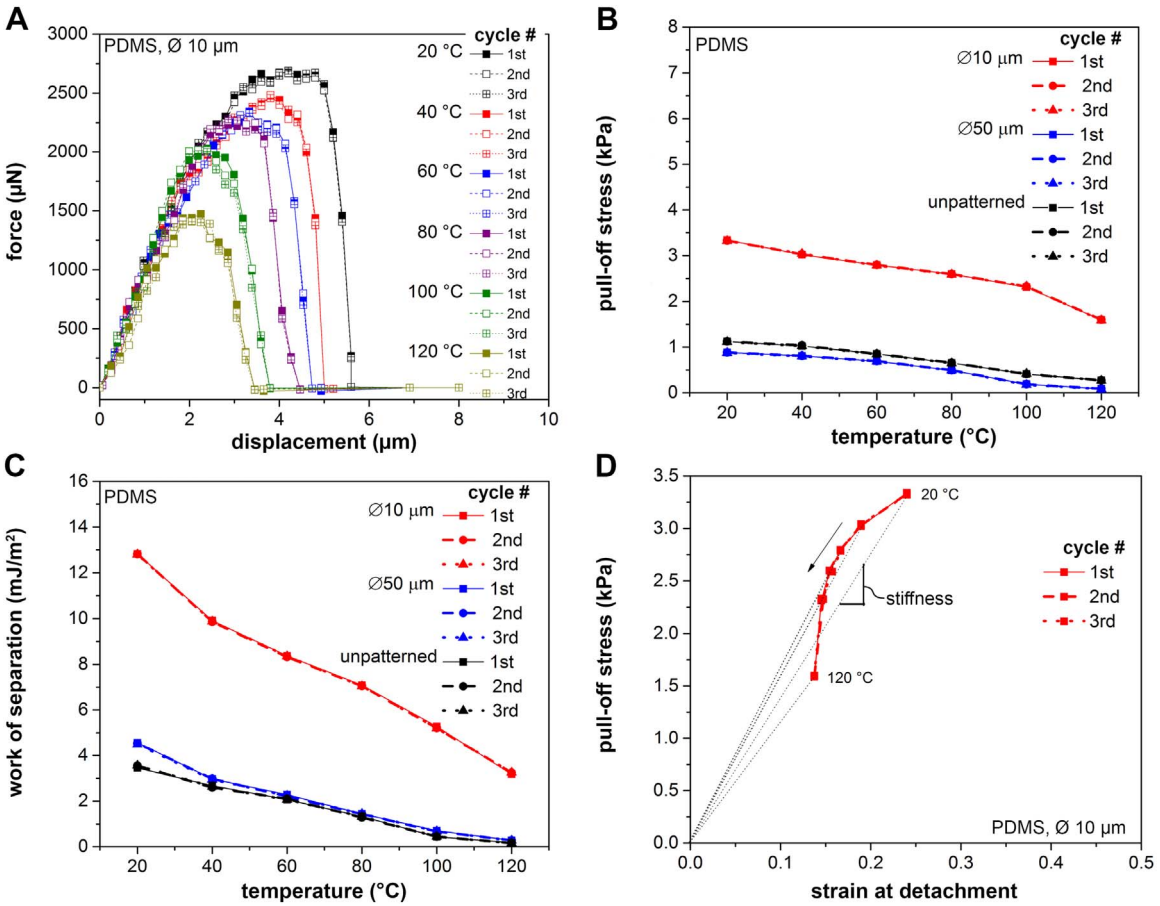

Fig. 2. Results of adhesion measurements of PDMS micropatterned specimens obtained from three heating-cooling cycles. (A) Force-displacement curves as a function of temperature for pillar structures with diameter 10 µm and aspect ratio 2. **(B)** Pull-off stresses and **(C)** work of separation as a function of temperatures, for the different micropatterned specimens (red: 10 µm pillar diameter, blue 50 µm pillar diameter) and an unpatterned control (black). **(D)** Pull-off stress in terms of the strain at detachment for pillar structures with diameter 10 µm at various temperatures. The slope of the secants (dotted lines) represents the apparent stiffness of the adhesives. (For interpretation of the references to color in this figure legend, the reader is referred to the web version of this article).

which is most likely due to the enhanced stiffness and reduced strain of the specimens (Fig. 4**d**). At low (20 °C) and high (100 and 120 °C) temperatures, in turn, the work of separation was fairly small with similar values for all samples in all cycles.

3.2. Dynamic mechanical material tests

To separate materials from structure effects, dynamic mechanical tests of the materials within the relevant temperature range were performed. The storage and loss modulus and the viscoelastic loss factor, $\tan\delta$, for all materials are presented in the Figs. 5–7 as a function of temperature. The material glass transition temperatures, T_g, obtained from the maxima in the $\tan\delta$ curves are summarized in Table 1. PDMS has the lowest glass transition temperature of −28 °C and PU-ht the highest T_g of 59 °C. For PFPEdma, two glass transition temperatures were identified at −20 °C and 27 °C (Fig. 6**a**). The viscoelastic loss factor, $\tan\delta$, was found to lie below 0.15 for PDMS and PFPEdma at temperatures above 20 °C (Figs. 5**b and** 6**b**). Hence, these materials can be considered as largely elastic, particularly at higher temperatures, where $\tan\delta$ was further reduced. The storage modulus of PDMS and PFPEdma decreased slightly with increasing temperature: For PDMS, it decreased from 2.7 MPa at 20 °C to 1.9 MPa at 120 °C (Fig. 5**b**); for PFPEdma, the storage modulus decreased from 10 MPa at 20 °C to 8.5 MPa at 60 °C and then remained almost constant at higher temperatures (Fig. 6**b**).

In contrast to PDMS and PFPEdma, the UV-cured polyurethane PU-ht is more viscoelastic exhibiting a viscoelastic loss factor of up to 3.3 at 59 °C (Fig. 7**a and b**). In addition, the storage modulus varied strongly from 50 MPa at 20 °C down to 2.5 MPa at 80 °C. Interestingly, the thermo-mechanical properties varied during the first heating cycle (Fig. 7**a and b**). Hereby, the material further stiffened as the storage modulus increased almost 10 times compared to the first cycle, most probably due to a secondary thermally induced cross-linking (referred to as post-bake, see Fig. 7**c and d**). In the same way, the material became less viscoelastic with a maximum $\tan\delta$ of about 0.3, i.e. one order of magnitude less compared to the initial viscoelasticity upon UV-curing (Fig. 7**d**). To exclude effects of morphological variations such as crystallization, XRD analysis was performed for PU-ht directly upon UV-curing and a subsequent post-bake at 120 °C. Upon both treatments, the diffraction patterns were found to be similar without any characteristic patterns due to crystalline domains (Fig. 8). The broad impulses at 2Θ=19. 8° demonstrate the amorphous microstructure of the polymers that did not vary by further cross-linking of the material. Thus, the results obtained indicate an amorphous morphology for both PU-ht samples without significant variations upon additional thermal cross-linking.

4. Discussion

The results presented in this paper showed that the adhesion properties of micropatterned polymer surfaces can depend significantly on temperature. The specimens made from PDMS and PFPEdma were operated at temperatures higher than their glass transition temperature. For both materials, the pull-off stress dropped in the order of about 50%

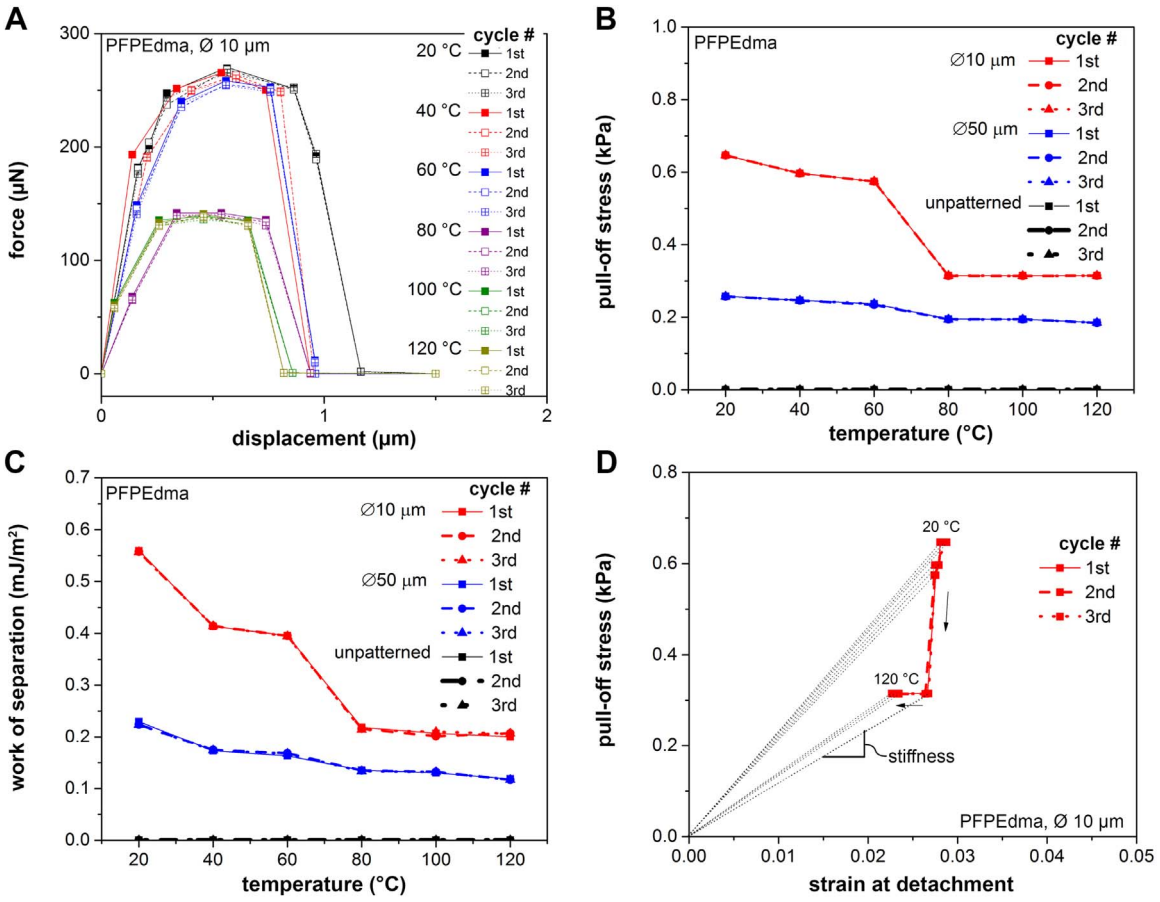

Fig. 3. Results of adhesion measurements of PFPEdma micropatterned specimens obtained from three heating-cooling cycles. (A) Force-displacement curves as a function of temperature for pillar structures with diameter 10 µm and aspect ratio 2. **(B)** Pull-off stresses and **(C)** work of separation as a function of temperatures, for the different micropatterned specimens (red: 10 µm pillar diameter, blue 50 µm pillar diameter) and an unpatterned control (black). **(D)** Pull-off stress in terms of the strain at detachment for pillar structures with diameter 10 µm at various temperatures. The slope of the secants (dotted lines) represents the apparent stiffness of the adhesives. (For interpretation of the references to color in this figure legend, the reader is referred to the web version of this article).

for a temperature elevation from 20 °C to 120 °C and completely recovered when cooled down to 20 °C again. In the same temperature regime, the viscoelastic loss factor, $\tan\delta$, decreased with increasing temperature for both materials. For PU-ht, the maximum pull-off stress was obtained at the temperature close to the glass transition, where the viscoelasticity of cross-linked elastomers is most pronounced. Viscoelasticity involves dissipative processes during detachment, which enhance the work of separation. This most likely explains the maximum at 60 °C for the patterned and unpatterned PU-ht specimens (Fig. 4c). Upon post-bake at 120 °C, however, the work of separation decreased due to an additional thermal cross-linking (only observed for PU-ht), resulting in a stiffer polymer network and a reduced viscoelastic loss factor (Fig. 7b) (Zosel, 1991). In contrast to the decrease in work of separation, the pull-off stress drastically increased with the stiffened structures. The reason lies in the fact that pull-off stress reflects the smaller contact area in the stiffer material. Thus, the stiffer structures led to higher adhesion, which is in line with earlier studies (Castellanos et al., 2011; Tang et al., 2005).

In addition to various degrees of viscoelasticity, the different surface free energies of the three tested polymers result in distinctive levels of adhesion. The highest pull-off stresses (of several ten kPa) were obtained with polyurethane (PU-ht); it has the highest surface energy of 42 mJ m^{-2} due to nonpolar and polar groups originating from diisocyanates and polyols. PDMS and PFPEdma are hydrophobic polymers with surface energies of 22 and 16 mJ m^{-2}, respectively (Hensel et al., 2012; Rolland et al., 2004). Particularly for PFPEdma, the high fluorine content (about 54 at%) and its high electron negativity make the material much less polarizable and, thus, reduce the probability for van der Waals interactions. This explains most probably the reduction of pull-off stress and the work of separation over two orders of magnitude compared to PU-ht (Zosel, 1985).

Of particular interest for adhesive devices is the effect of surface micropatterning on adhesive performance. Our study confirms earlier results that surface micropatterning can significantly enhance adhesion over unpatterned controls, which were much less adhesive or even non-adhesive (see results for PFPEdma). However, micropatterning *per se* does not always lead to higher adhesion. For PDMS and PU-ht, only the smallest pillar structures (diameter 10 µm, aspect ratio 2) were more adhesive than the unpatterned control (in terms of pull-off stresses). By contrast, the coarser pillar structures with aspect ratio 0.4 were always inferior to the finer pillar structures with aspect ratio 2 and, for PDMS and PU-ht, even to the unpatterned samples. The explanation lies in the fact that micropatterning, at first, creates adhesive structures with a trivial geometric disadvantage: it invariably reduces the nominal contact area compared to an ideal unpatterned contact; this penalty needs to be overcome by the adhesion-enhancing contact splitting effects, which require good contact formation and small elastic strain energy build-up. It stands to reason that, all other things being equal, the pillar aspect ratio will decide whether a micropatterned surface is anti-adhesive (inferior to an unpatterned control) or adhesive (superior to an unpatterned contact). A higher aspect ratio results in a lower effective stiffness of a patterned structure, which typically results in better contact formation and reduced elastic strain energy for a given strain value (Spolenak et al., 2005). At a critical value of the aspect ratio (in our study between 0.4 and 2), the geometric disadvantage is overruled, rendering an adhesive micropattern. The actual contact area

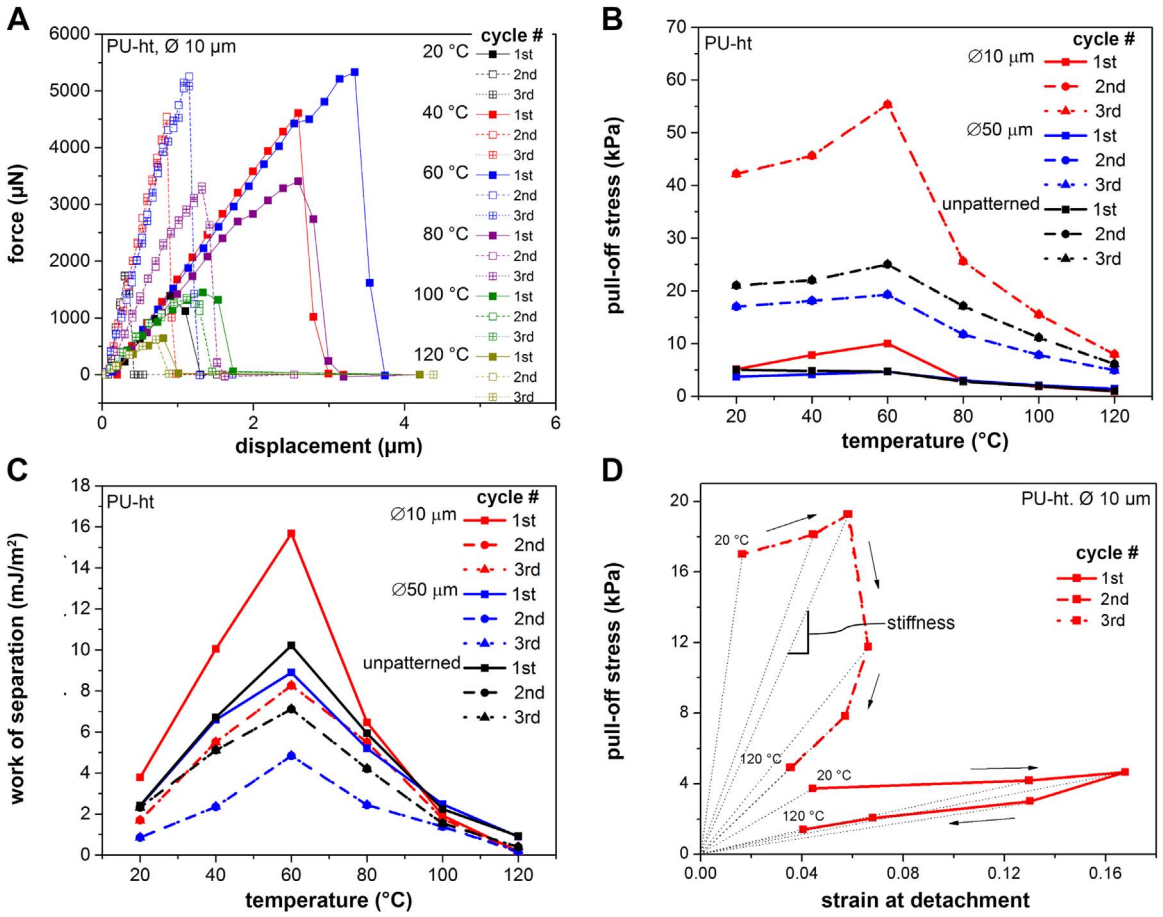

Fig. 4. Results of adhesion measurements of PU-ht micropatterned specimens obtained from three heating-cooling cycles. (A) Force-displacement curves as a function of temperature for pillar structures with diameter 10 µm and aspect ratio 2. **(B)** Pull-off stresses and **(C)** work of separation as a function of temperatures, for the different micropatterned specimens (red: 10 µm pillar diameter, blue 50 µm pillar diameter) and an unpatterned control (black). **(D)** Pull-off stress in terms of the strain at detachment for pillar structures with diameter 10 µm at various temperatures. The slope of the secants (dotted lines) represents the apparent stiffness of the adhesives. (For interpretation of the references to color in this figure legend, the reader is referred to the web version of this article).

further correlates with the flexibility to bend and to adapt to the spherical probe, which increases with the length of the pillars (Castellanos et al., 2011). In addition to that, the amount of dissipated energy during pull-off scales linearly with the length of the pillar (Jagota and Bennison, 2002). Therefore, pillar structures with higher aspect ratio are more adhesive as demonstrated in our results for all tested materials in accordance to literature (Greiner et al., 2007; Spolenak et al., 2005).

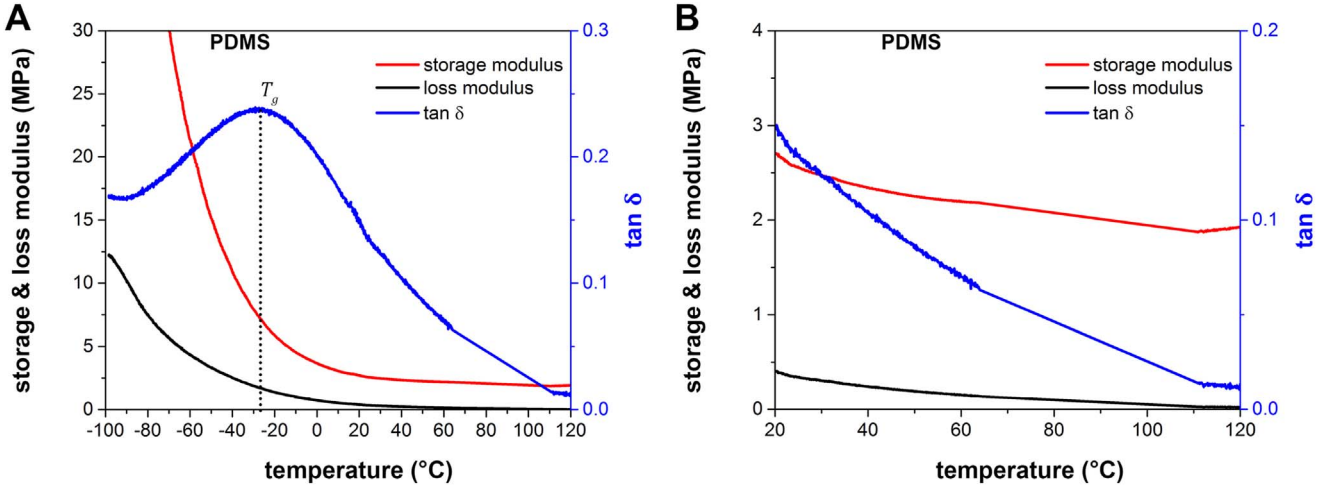

Fig. 5. Results of dynamic mechanical tests of bulk PDMS. The storage modulus (red), loss modulus (black), and the viscoelastic loss factor, tan δ (blue), are plotted as a function of temperature. The glass transition temperature is determined from the maximum value of tan δ as highlighted with the dotted line. **(A)** Temperature range of the DMTA from −100 °C to 120 °C. **(B)** Temperature range of the adhesion measurements from 20 °C to 120 °C. (For interpretation of the references to color in this figure legend, the reader is referred to the web version of this article).

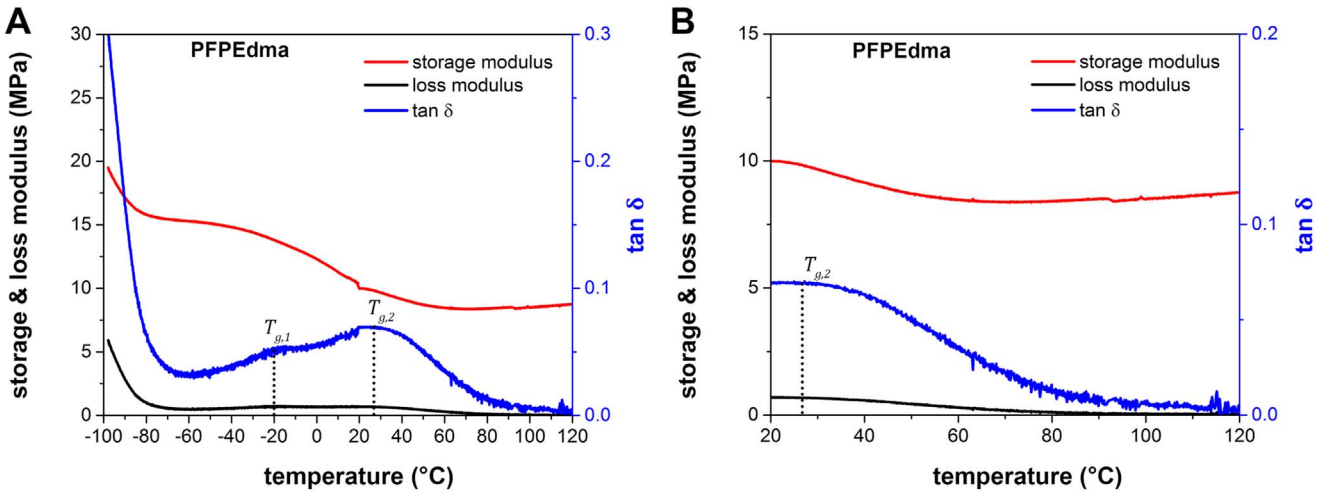

Fig. 6. Results of dynamic mechanical tests of bulk PFPEdma. The storage modulus (red), loss modulus (black), and the viscoelastic loss factor, tan δ (blue), are plotted as a function of temperature. The glass transition temperatures are determined from the maximum value of tan δ as highlighted with the dotted line. **(A)** Temperature range of the DMTA from −100 °C to 120 °C. **(B)** Temperature range of the adhesion measurements from 20 °C to 120 °C. (For interpretation of the references to color in this figure legend, the reader is referred to the web version of this article).

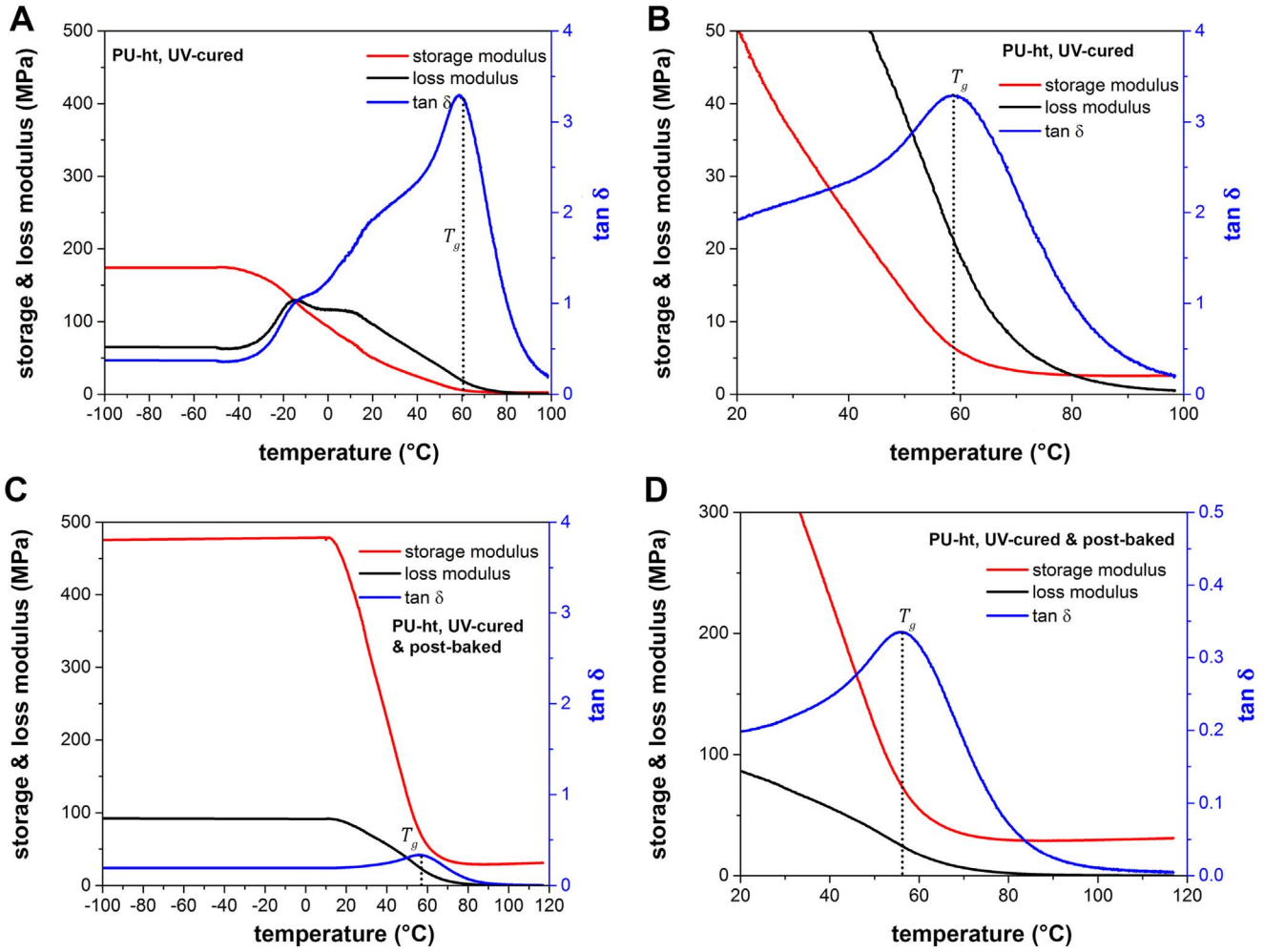

Fig. 7. Results of dynamic mechanical tests of bulk PU-ht. The storage modulus (red), loss modulus (black), and the viscoelastic loss factor, tan δ (blue), are plotted as a function of temperature. The glass transition temperature is determined from the maximum value of tan δ as highlighted with the dotted line. **(A,B)** DMTA trace of PU-ht upon UV-curing: **(A)** Temperature range of the DMTA from −100 °C to 100 °C. **(B)** Temperature range of the adhesion measurements from 20 °C to 100 °C. **(C,D)** DMTA trace of PU-ht upon UV-curing and subsequent post-bake at 120 °C: **(C)** Temperature range of the DMTA from −100 °C to 120 °C. **(D)** Temperature range of the adhesion measurements from 20 °C to 120 °C. (For interpretation of the references to color in this figure legend, the reader is referred to the web version of this article).

Table 1
The material glass transition temperatures (T_g) and surface free energies (γ).

Polymer	T_g (°C)	γ (mJ m^{-2})
PDMS	−28	22 [40]
PFPEdma	−20 & 27	16 [34]
PU-ht	59	42

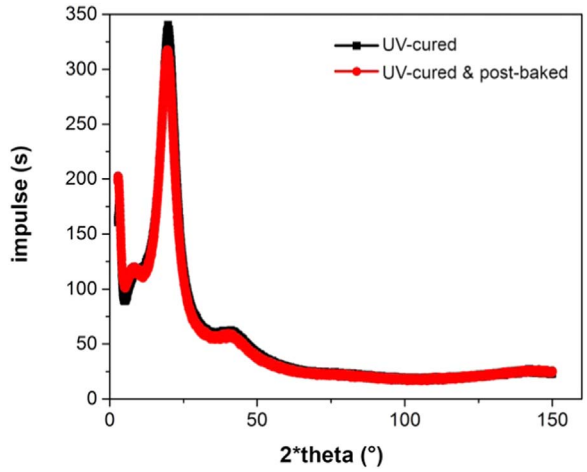

Fig. 8. XRD analysis of PU-ht immediately upon UV-curing (black squares) and after subsequent post-bake at 120 °C (red circles). (For interpretation of the references to color in this figure legend, the reader is referred to the web version of this article).

5. Conclusions

In this paper, we presented a detailed study on the impact of temperatures on three different polymeric, micropatterned adhesives. We demonstrated that the adhesion is enhanced by the viscoelastic characteristics of the materials and the surface micropatterning. The glass transition temperature was identified as the temperature of maximum adhesion due to the peak in the viscoelastic loss factor. The following conclusions were drawn:

- The pull-off stress and the work of separation critically depend on the temperature as found for three different materials, namely, PDMS, PFPEdma, and PU-ht. For PDMS and PFPEdma, both quantities monotonically decreased with increasing temperature; whereas for PU-ht, the pull-off stress and the work of separation exhibit maxima at 60 °C.
- Viscoelastic contributions alter adhesion in terms of the work of separation. To take advantage of this effect, the operating temperature of an adhesive should be chosen close to the material glass transition temperature for maximum performance.
- The adhesion performance strongly varies close to the glass transition temperature. Hence, for a reliable, predictable adhesion performance over a certain temperature range, the glass transition temperature should be avoided.
- The adhesion is higher for materials with higher surface free energy. To enhance the intrinsic adhesion by micropatterning, pillars with an adequate length to adapt to curved substrates are necessarily required.
- It must be noticed that cross-linking of PU-ht by UV-exposure was not sufficient to generate the complete polymer network. Only upon post-bake at 120 °C were the structures completely cross-linked. Such a two-step cross-linking procedure might open ways to create tunable or even switchable adhesives.

Taken together, the temperature-dependent viscoelasticity of elastomers has a strong impact on adhesion and is different for varying temperatures. Hence, the temperature needs to be considered carefully in the material selection and the technical design of micropatterned adhesive devices.

Acknowledgements

We thank Jennifer Dollmann and Marlon Jochum for the dynamical mechanical thermal analysis, Rudolf Karos for his help on X-ray diffraction analysis. The research leading to these results has received funding from the European Research Council under the European Union's Seventh Framework Programme (FP/2007-2013)/ERC Grant Agreement n. 340929 and by the Leibniz-Competition Grant n. 493.

References

Andrews, E.H., Kinloch, A.J., 1973. Mechanics of adhesive failure. II. Proc. R. Soc. Lond. A. Math. Phys. Sci. 332, 401–414.
Arzt, E., Gorb, S., Spolenak, R., 2003. From micro to nano contacts in biological attachment devices. Proc. Natl. Acad. Sci. USA 100, 10603–10606.
Awada, H., Noel, O., Hamieh, T., Kazzi, Y., Brogly, M., 2011. Contributions of chemical and mechanical surface properties and temperature effect on the adhesion at the nanoscale. Thin Solid Films 519, 3690–3694.
Balijepalli, R.G., Fischer, S.C.L., Hensel, R., McMeeking, R.M., Arzt, E., 2017. Numerical study of adhesion enhancement by composite fibrils with soft tip layers. J. Mech. Phys. Solids 99, 357–378.
Barquins, M., Maugis, D., 1981. Tackiness of elastomers. J. Adhes. 13, 53–65.
Barreau, V., et al., 2016. Fibrillar elastomeric micropatterns create tunable adhesion even to rough surfaces. Adv. Funct. Mater. Mater. 26, 4687–4694.
Camino, C., Lomakin, S.M., Lazzari, M., 2001. Polydimethylsiloxane thermal degradation part 1. Kinetic aspects. Polymer 42, 2395–2402.
Cappella, B., Stark, W., 2006. Adhesion of amorphous polymers as a function of temperature probed with AFM force-distance curves. J. Colloid Interface Sci. 296, 507–514.
Castellanos, G., Arzt, E., Kamperman, M., 2011. Effect of viscoelasticity on adhesion of bioinspired micropatterned epoxy surfaces. Langmuir 27, 7752–7759.
Cheung, E., Sitti, M., 2009. Adhesion of biologically inspired polymer microfibers on soft surfaces. Langmuir 25, 6613–6616.
Crosby, A.J., Shull, K.R., 1999. Adhesive failure analysis of pressure-sensitive adhesives. J. Polym. Sci. Part B Polym. Phys. 37, 3455–3472.
Del Campo, A., Greiner, C., Arzt, E., 2007. Contact shape controls adhesion of bioinspired fibrillar surfaces. Langmuir 23, 10235–10243.
Fischer, S.C.L., Arzt, E., Hensel, R., 2017. Composite pillars with tuneable interface for adhesion to rough substrates. ACS Appl. Mater. Interfaces 9, 1036–1044.
Greenwood, J.A., Johnson, K.L., 1981. The mechanics of adhesion of viscoelastic solids. Philos. Mag. A 43, 697–711.
Greiner, C., Del Campo, A., Arzt, E., 2007. Adhesion of bioinspired micropatterned surfaces: effects of pillar radius, aspect ratio, and preload. Langmuir 23, 3495–3502.
Greiner, C., Spolenak, R., Arzt, E., 2009. Adhesion design maps for fibrillar adhesives: the effect of shape. Acta Biomater. 5, 597–606.
Hensel, R., et al., 2012. Free-floating hydrogel-based rafts supporting a microarray of functional entities at fluid interfaces. Soft Matter 8, 5293–5300.
Hensel, R., et al., 2014. In situ experiments to reveal the role of surface feature sidewalls in the Cassie-Wenzel transition. Langmuir 30, 15162–15170.
Jagota, A., Bennison, S.J., 2002. Mechanics of adhesion through a fibrillar microstructure. Integr. Comp. Biol. 42, 1140–1145.
Kamperman, M., Kroner, E., Del Campo, A., McMeeking, R.M., Arzt, E., 2010. Functional adhesive surfaces with 'Gecko' effect: the concept of contact splitting. Adv. Eng. Mater. 12, 335–348.
Kendall, K., 1971. The adhesion and surface energy of elastic solids. J. Phys. D. Appl. Phys. 4, 1186–1195.
Khaderi, S.N., Fleck, N. a, Arzt, E., McMeeking, R.M., 2015. Detachment of an adhered micropillar from a dissimilar substrate. J. Mech. Phys. Solids 75, 159–183.
Kim, S., Aksak, B., Sitti, M., 2007. Enhanced friction of elastomer microfiber adhesives with spatulate tips. Appl. Phys. Lett. 91.
Kroner, E., Arzt, E., 2012. Single macropillars as model systems for tilt angle dependent adhesion measurements. Int. J. Adhes. Adhes. 36, 32–38.
Lakhera, N., et al., 2013. Adhesion behavior of polymer networks with tailored mechanical properties using spherical and flat contacts. MRS Commun. 3, 73–77.
Luengo, G., Pan, J., Heuberger, M., Israelachvili, J.N., 1998. Temperature and time effects on the 'adhesion dynamics' of poly(butyl methacrylate) (PBMA) surfaces. Langmuir 14, 3873–3881.
Murphy, M.P., Aksak, B., Sitti, M., 2007. Adhesion and anisotropic friction enhancements of angled heterogeneous micro-fiber arrays with spherical and spatula tips. J. Adhes. Sci. Technol. 21, 1281–1296.
Noy, A., Zepeda, S., Orme, C.A., Yeh, Y., De Yoreo, J.J., 2003. Entropic barriers in nanoscale adhesion studied by variable temperature chemical force microscopy. J. Am. Chem. Soc. 125, 1356–1362.
Purtov, J., Frensemeier, M., Kroner, E., 2015. Switchable adhesion in vacuum using bio-inspired dry adhesives. ACS Appl. Mater. Interfaces 7, 24127–24135.
Rolland, J.P., Hagberg, E.C., Denison, G.M., Carter, K.R., De Simone, J.M., 2004. High-resolution soft lithography: enabling materials for nanotechnologies. Angew. Chem. –

Int. Ed. 43, 5796–5799.
Shull, K.R., 2002. Contact mechanics and the adhesion of soft solids. Mater. Sci. Eng.: R: Rep. 36, 1–45.
Spolenak, R., Gorb, S., Arzt, E., 2005. Adhesion design maps for bio-inspired attachment systems. Acta Biomater. 1, 5–13.
Tang, T., Hui, C.-Y., Glassmaker, N.J., 2005. Can a fibrillar interface be stronger and tougher than a non-fibrillar one? J. R. Soc. Interface 2, 505–516.
Tsui, O.K.C., Wang, X.P., Ho, J.Y.L., Ng, T.K., Xiao, X., 2000. Studying surface glass-to-rubber transition using atomic force microscopic adhesion measurements. Macromolecules 33, 4198–4204.
Turi, E., 2012. Thermal Characterization of Polymeric Materials. Elsevier, New York.
Wu, S., 1973. Polar and nonpolar interactions in adhesion. J. Adhes. 5, 39–55.
Yu, H., Li, Z., Jane Wang, Q., 2013. Viscoelastic-adhesive contact modeling: application to the characterization of the viscoelastic behavior of materials. Mech. Mater. 60, 55–65.
Zeng, H.B., Maeda, N., Chen, N.H., Tirrell, M., Israelachvili, J., 2006. Adhesion and friction of polystyrene surfaces around T(g). Macromolecules 39, 2350–2363.
Zhou, M., et al., 2013. Controllable interfacial adhesion applied to transfer light and fragile objects by using gecko inspired mushroom-shaped pillar surface. ACS Appl. Mater. Interfaces 5, 10137–10144.
Zosel, A., 1985. Adhesion and tack of polymers: influence of mechanical properties and surface tensions. Colloid Polym. Sci. 263, 541–553.
Zosel, A., 1991. Effect of cross-linking on tack and peel strength of polymers. J. Adhes. 34, 201–209.